Effects of Desingularization and Collocation-Point Shift on Steady Waves with Forward Speed

Yonghwan Kim* & Dick K.P. Yue**
Massachusetts Institute of Technology, Department of Ocean Engineering, Cambridge, MA, USA
* ykim@vfrl.mit.edu, **yue@mit.edu

Introduction

After the pioneering work of Dawson ([1]) for steady ship waves, many variations of panel method have been studied for steady ship wave problems. In the early stage of those studies, the application to wave-resistance computation was of primary interest for practical reasons, and such studies contributed to the births of some computer programs, e.g. DAWSON, SHIPFLOW, SWIFT and RAPID. Sclavounos and Nakos ([2]) introduced a strong background of the Rankine panel method based on a rigorous stability analysis for steady wave problems, and also showed the advantage of the higher-order B-spline scheme. Raven ([3]) introduced the favorable properties of a raised-panel method using the similar two-dimensional stability analysis, and Bunnik ([4]) also included the effects of raising panel in his unsteady stability analysis. In the present study, theoretical and numerical efforts are given to observe the effects of desingularization and collocation-point shift on the numerical solution of panel method. We perform a more complete three-dimensional stability analysis, and a numerical error is defined to compare the accuracy of different numerical schemes. For validating our theoretical analysis, the numerical solutions of steady wave problem near a point singularity with forward speed are observed.

Stability Analysis of Steady Rankine Panel Method

The linear free surface boundary condition with a steady forward speed U is written as

$$U^2 \frac{\partial^2 \Phi}{\partial x^2} + g \frac{\partial \Phi}{\partial z} = 0 \quad . \tag{1}$$

When the free surface is discretized into uniform rectangular panels of the size $(\Delta x, \Delta y)$, the disturbed free-surface flow (potential Φ or singularity strength σ) in a discrete domain can be written as

$$\begin{pmatrix} \Phi \\ \sigma \end{pmatrix} = \frac{1}{(2\pi)^2} \int_{-\pi/\Delta x}^{\pi/\Delta x} \int_{-\pi/\Delta y}^{\pi/\Delta y} \frac{\hat{R}}{\hat{W}} e^{-i(ul\Delta x + vm\Delta y)}\, du dv \ . \tag{2}$$

$\hat{W}$ includes the numerical dispersion relation. At first, let's consider a constant source distribution method such that

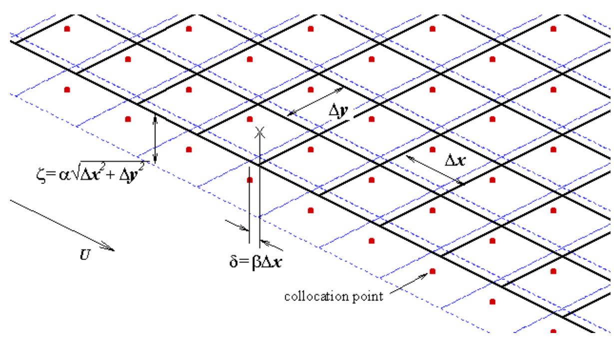

Figure 1. Definitions for stability analysis

$$U^2 \frac{\partial^2}{\partial x^2} \sum_l \sigma_l \int_l \frac{1}{R} dS + g \frac{\partial}{\partial z} \sum_l \sigma_l \int_l \frac{1}{R} dS = 0 \tag{3}$$

where *1/R* is the distance between the field and singularity points. Omitting the details, $\hat{W}$ corresponding equation (3) can be written as follows:

$$\hat{W} = \hat{D}\hat{I}_x + k_0 \hat{I}_z \tag{4}$$

where $k_0 = g/U^2$, and

$$\hat{D} = \sum_{j=-J1}^{J2} \frac{d_j}{\Delta x} e^{i(j\Delta x u)} \tag{5}$$

$$\hat{I}_x = \sum_m \sum_n 2\pi i u_m \frac{e^{(z-\varsigma)\sqrt{u_m^2+v_m^2} + iu_m\delta}}{\sqrt{u_m^2+v_m^2}} \left\{ \frac{\sin(u_m \Delta x/2)}{u_m \Delta x/2} \right\}^{p+1} \left\{ \frac{\sin(v_n \Delta y/2)}{v_n \Delta y/2} \right\}^{q+1} \tag{6}$$

$$\hat{I}_z = \sum_m \sum_n -2\pi e^{(z-\varsigma)\sqrt{u_m^2+v_m^2}+iu_m\delta} \left\{\frac{\sin(u_m \Delta x/2)}{u_m \Delta x/2}\right\}^{p+1} \left\{\frac{\sin(v_n \Delta y/2)}{v_n \Delta y/2}\right\}^{q+1} \tag{7}$$

where $u_m = u + 2\pi m/\Delta x$, $v_n = v + 2\pi n/\Delta y$, and *p=q=0*. $\varsigma\,(=\alpha\sqrt{\Delta x^2+\Delta y^2})$ is the height of panel surface raised from the free surface and $\delta\,(=\beta\Delta x)$ is the longitudinal shift of collocation points. $\hat{D}$ is the discrete Fourier transform of finite difference, and d_j's are the corresponding coefficients. For example, the Dawson's 4-point difference is the case that *J1=0*, *J2=4*, and d_j=10/6, -15/6, 1, -1/6. The higher-order B-spline source distribution provides a similar dispersion relation, but $\hat{D}$ is not necessary and the order of the spline function can be controlled by *p* and *q* in equation (6) and (7). For instance, *p=q=2* indicates a bi-quadratic distribution. In addition, $\hat{I}_x$ should be replaced to $iu_m\hat{I}_x$. In the case of a potential-based method, the discrete Fourier transform of the Green's 2nd identity should be observed and the desingularization is not applicable. For the potential-based method, the details are well described in [2].

Figure 2 shows the numerical dispersion and damping of the source methods with different α and β, and three different schemes are considered. The *x*-axis in this figure is the exact wave number, and the *y*-axes are the wave number to appear in actual computation and damping coefficient relative to the corresponding waves. Therefore, the schemes of figure (a) and (b) can provide one or two numerical wave components depending on Δx, and no solution is also possible. $u_0\Delta x/2\pi$ has a range of 1/40~1/10 in most practical computation, and the saw-tooth wave may appear in this range. As expected, the numerical damping increases when the collocation points are shifted to upstream. The numerical damping shown here is more thoroughly studied by Kim and Yue ([5]). On the other hand, the desingularization induces longer wavelength than the conventional method. These results are consistent with the two-dimensional cases of Raven ([3]). α and β do not affect much the higher-order scheme, except for a small damping due to nonzero β. In a practical point of view, $u_0\Delta x/2\pi$ less than 0.1 is of great importance.

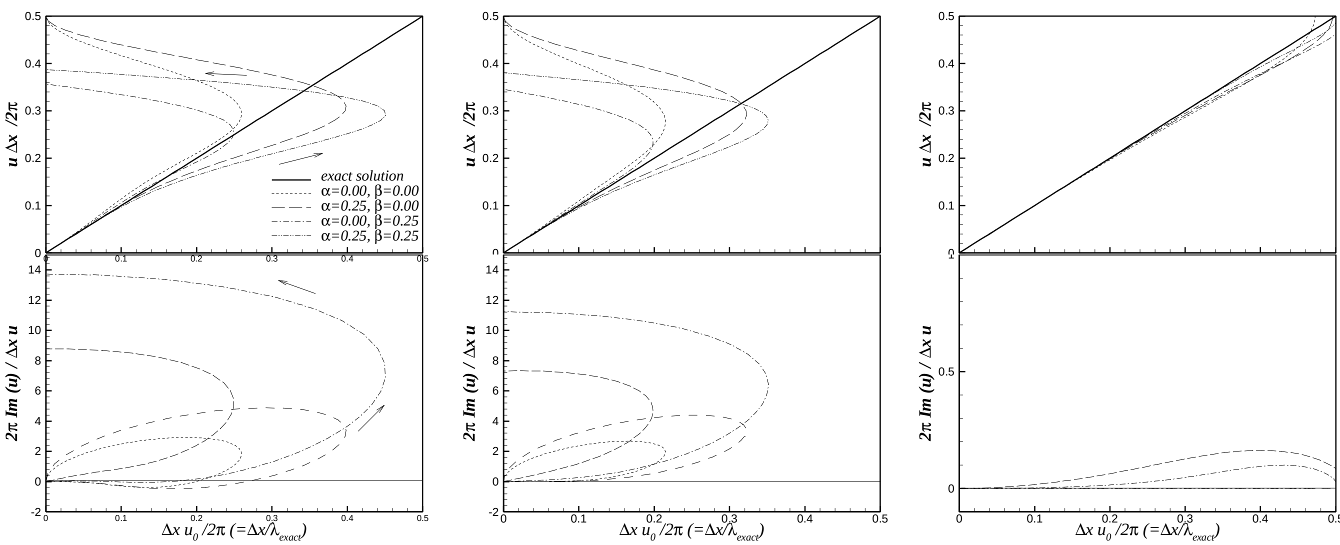

(a) 4-point conventional (b) 4-point Dawson (c) Bi-quadratic B-spline

Figure 2. Numerical dispersion and damping for different α and β : source method, α =0, 0.25, β =0, 0.25, $\Delta x/\Delta y = 1$

Numerical Errors

Two major sources of computational error are dispersion error, and numerical damping. The dispersion error causes the difference of wavelength, and the numerical damping causes the difference of wave amplitude. To observe the overall accuracy of a certain numerical scheme, we define a parameters such that

$$E_\gamma^{(m,N)} = \int_0^\gamma \frac{\int_0^{\Delta x/\tilde{u}_0} |\, e^{i\tilde{u}_0 x} - e^{i\tilde{u} x}\,|^m \, dx}{N\Delta x/\tilde{u}_0} \frac{1}{\tilde{u}}\, d\tilde{u} \tag{11}$$

where $\tilde{u} = u\Delta x / 2\pi$ and u_0 is the exact wave number. $E_\gamma^{(m,N)}$ is an integral of weighted numerical errors in a range of $0 \le \tilde{u} \le \gamma$ over N wavelengths. $\tilde{u} = 1/2$ is the maximum discrete wave number to possibly appear, and this wave is so-called saw-tooth wave which is not desirable in the viewpoint of numerical stability. $1/\tilde{u}$ in (11) is multiplied to give more weight when $\tilde{u}$ is small. It should be noted that the consistency of a numerical scheme implies that the numerator of (11) should vanish as $\tilde{u}$ approaches zero. $E_\gamma^{(m,N)}$ reflects a limited damping effects at large $\tilde{u}$, but may be a good index to compare the overall errors in a specific range of $\tilde{u}$.

Figure 3 compares $E_{0.1}^{(1,2)}$ and $E_{0.1}^{(1,6)}$ for different numerical schemes. This result can be particularly important in a practical perspective, since $\gamma \le 0.1$ is valid in most numerical computations. According to this result, the desingularization method seems to reduce the overall numerical error, and the optimum case depends on the numerical scheme. The 3-point and Dawson's difference have an optimum α near 0.2. On the other hand, the higher-order method does not have a significant benefit. The effect of collocation-point shift is not significant in this case. The 4-point conventional difference scheme has some reduction of error due to the numerical damping compensating the negative damping in this range of γ (see Figure 2-(a)).

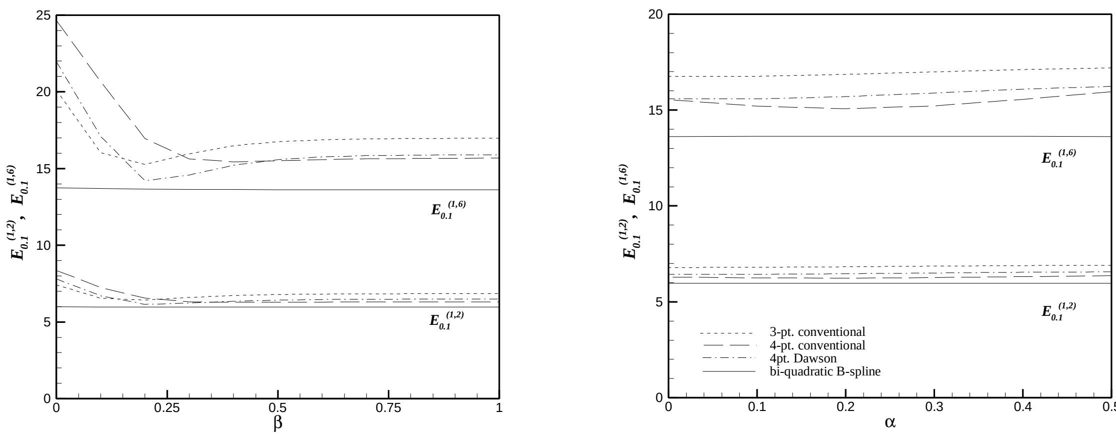

(a) α =0 (b) β =0,0.25

Figure 3. $E_{0.1}^{(1,2)}$ and $E_{0.1}^{(1,6)}$ of four numerical schemes; source method; $\Delta x / \Delta y = 1$

Applications and Validation

The steady wave elevations near a moving point singularity located at (x,y,z)=(0,0,-d) are obtained using a few different numerical schemes to validate the stability and error analyses. In this computation, $U/\sqrt{gd}$ =1.0 is applied, and the computational domain covers 1.5 (upstream) and 3.5 (downstream) times of exact wavelength in longitudinal direction and twice in transverse direction. The numbers of applied grids are 50x20 ($\tilde{u}_0 = 1/10$), 70x30 ($\tilde{u}_0 = 1/15$) and 100x20 ($\tilde{u}_0 = 1/20$). Figure 4 compares the wave elevations at y/d=1.0 for different α and β. As expected, shorter waves are observed in the conventional scheme, i.e. when α =0 and β =0. However, the wavelengths are longer in the case of nonzero α. Also significant damping is shown for nonzero β. Figure 5 is the elevation contour plots of three solutions, showing slightly different wave angles. A larger angle is found when α =0 and β =0, but the solution obtained from the desingularized scheme shows an excellent agreement with the analytic solution. To understand this trend, we should observe both the longitudinal and transverse wave numbers, (u,v), as shown in Figure 6. Figure 6 shows the three-dimensional surfaces of (u_0, u, v) for the two cases of Figure 5. For a given exact wave number (u_0) and Δx (e.g. bold line on bottom), the conventional method induces smaller u and larger v (contour on upper surface) than the desingularized case (contour on lower surface). This causes shorter longitudinal waves and longer transverse wave, consequently the larger wave angle. Figure 7 compares the numerical errors obtained from the source method and $E_{0.5}^{(1,4)}$ predicted by the stability analysis. The numerical errors obtained from the source method is defined as follows:

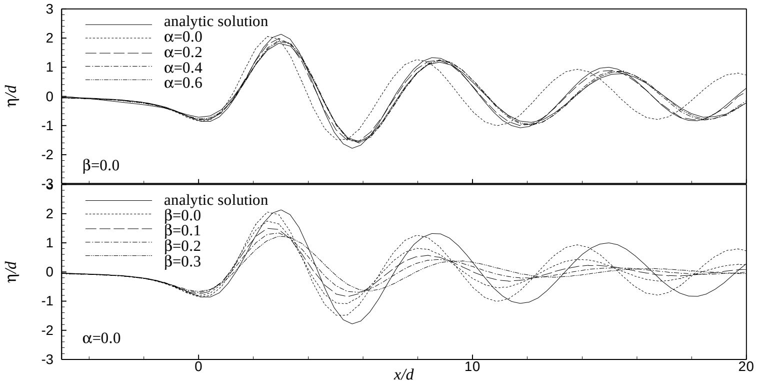

Figure 4. Wave elevations at *y/d*=1.0; 4-pt. Dawson, 75x30 grids

$$E_{RSM} = \frac{\int_S |\eta_0 - \eta|\, ds}{\text{domain area}\,(S)} \qquad (12)$$

where η_0 is the wave elevation of exact solution. Although the magnitudes of two errors are not same (because of different definitions), they show a fair agreement of the sensitivity on α and β. Similar to Figure 3, the minimum errors are found near β=0.2 in both cases.

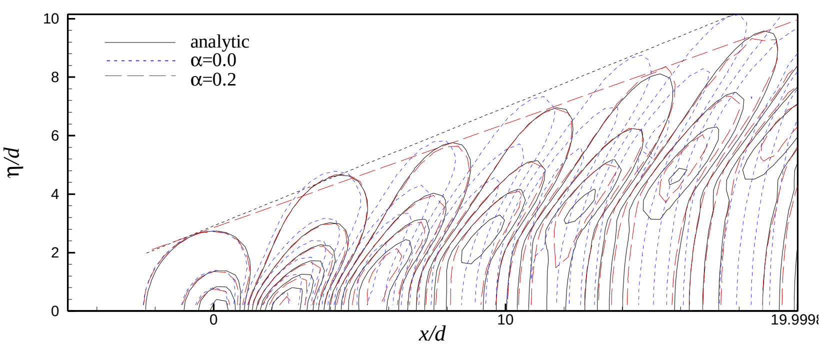

Figure 6. Wave contours near a moving sink: β=0.0, 100x20 grids

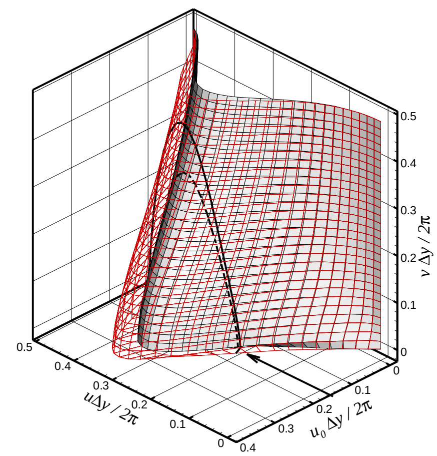

Figure 6. (u_0, *u*, *v*) surface for two cases of Figure 5.

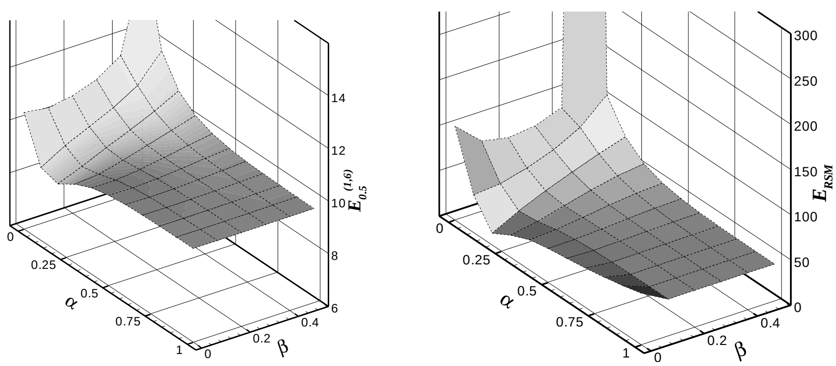

(a) $E_{0.5}^{(1,4)}$ (b) Actual error

Figure 7. $E_{0.5}^{(1,4)}$ and actual elevation error; 75x30 grids

References

[1] Dawson,, C.W. 1977 Proc. 2nd Int. Conf. Numerical Ship Hydrodynamics.

[2] Sclavounos, P.D. & Nakos, D.E. 1998 Proc. 17th Symp. Naval Hydrodynamics.

[3] Raven, H.C. 1996 PhD. Dissertation, Delft University of Technology.

[4] Bunnik, T. 1999 PhD. Dissertation, Delft University of Technology.

[5] Kim, Y. & Yue, D.K.P. 2003 8th Conf. Numerical Ship Hydrodynamics (submitted)

Question by : X.B. Chen

Thank you for your important work which helps me to understand the difficulty of R.P.M. in modelling surface waves. My question is whether you've studied as well such effects on global values such as the wave resistance which are associated with wave patterns, and how much are they?

Author's reply:

There is no doubt that computational parameters such as desingularization and collocation point shift affect the wave resistance predictions. The degree this is true depends on physical parameters such as geometry and speed. For example, Fig. A shows significant difference of wave contours around a Wigley hull obtained with and without desingularization and collocation-point shift. We are in the process of obtaining more systematic data on the wave resistance and look forward to publishing these when they are available

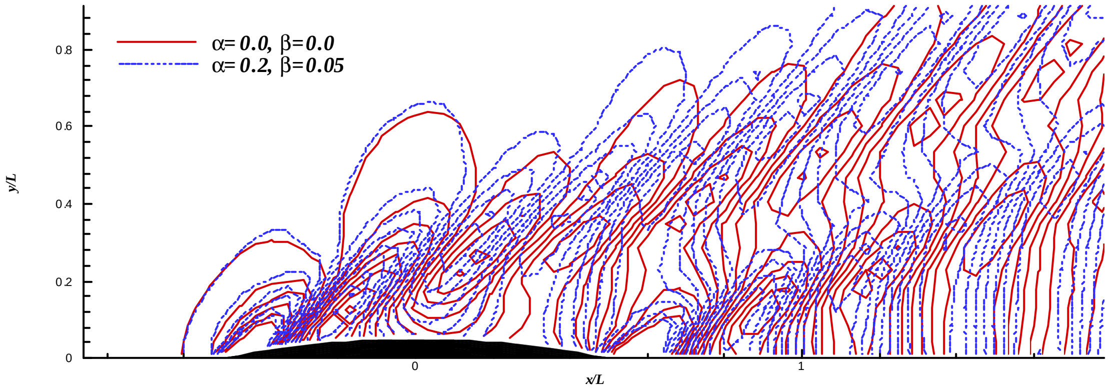

Fig. A comparison of wave contours around Wigley Hull at Froude number 0.3
